

# On the exact limit of the time-dependent coupled cluster ansatz and its approximations in the real-time equation-of-motion coupled cluster cumulant Green's function approach

Bo Peng,<sup>1, a)</sup> Himadri Pathak,<sup>1</sup> Ajay Panyala,<sup>2</sup> Fernando D. Vila,<sup>3</sup> John J. Rehr,<sup>3</sup> and Karol Kowalski<sup>1</sup>

<sup>1)</sup>*Physical and Computational Science Directorate, Pacific Northwest National Laboratory, Richland, Washington, 99354, USA*

<sup>2)</sup>*Advanced Computing, Mathematics, and Data Division, Pacific Northwest National Laboratory, Richland, Washington 99354, USA*

<sup>3)</sup>*Department of Physics, University of Washington, Seattle, WA 98195*

(Dated: June 4, 2024)

In this paper, we analyze the properties of the recently proposed real-time equation-of-motion coupled-cluster (RT-EOM-CC) cumulant Green's function approach [J. Chem. Phys. 2020, 152, 174113]. We specifically focus on identifying the limitations of the original time-dependent coupled cluster (TDCC) ansatz and propose an enhanced extended TDCC ansatz ensuring the exactness in the expansion limit. Additionally, we introduce a practical cluster-analysis-based approach for characterizing the peaks in the computed spectral function from the RT-EOM-CC cumulant Green's function approach, which is particularly useful for the assignments of satellite peaks when many-body effects dominate the spectra. Our preliminary numerical tests focus on reproducing, approximating, and characterizing the exact impurity Green's function of the three-site and four-site single impurity Anderson models using the RT-EOM-CC cumulant Green's function approach. The numerical tests allow us to have a direct comparison between the RT-EOM-CC cumulant Green's function approach and other Green's function approaches in the numerical exact limit.

## I. INTRODUCTION

Attosecond laser pulses exhibit a broad spectral range and relatively high intensity, pioneering ultrafast research such as delayed photoemission,<sup>1-3</sup> electronic response to sudden ionization,<sup>4-6</sup> charge localization and transfer in molecules,<sup>7,8</sup> autoionization absorption,<sup>9</sup> and conductivity control in dielectrics,<sup>10</sup> to name a few. Typically, in instantaneous processes lasting up to a few femtoseconds, the electronic dynamics can be considered free from nuclear motion, allowing theoretical treatments to focus solely on solving the time-dependent electronic Schrödinger equation within the Born-Oppenheimer approximation, which directly corresponds to experimental setups. Various time-dependent electronic structure methods have been developed in both the frequency and time domains. For example, real-time time-dependent density-functional theory<sup>11</sup> often demonstrates a reasonable balance between computational efficiency and accuracy. Nevertheless, for dynamics of the electronic excited states that feature strong electron correlation and often involve multiple configurations, multi-configurational time-dependent Hartree-Fock methods<sup>12-14</sup> or active space self-consistent field methods<sup>15-17</sup> can be employed for higher accuracy, albeit with very demanding computational costs. Alternative high-level approaches that exhibit modest polynomial scaling with the capability of systematic improvement in accuracy usually focus on time-dependent coupled cluster (TDCC) theory.<sup>18-20</sup> Previous efforts have demonstrated the capability of the TDCC formulation in identifying excitation energy,<sup>21</sup> computing linear response properties,<sup>19</sup> computing spectral functions<sup>22</sup> and linear absorption spectra in ultraviolet and X-ray energy regimes,<sup>23-26</sup> including the incorporation of relativistic

wave functions,<sup>27</sup> finite temperature and non-equilibrium formalism,<sup>28,29</sup> reduced scaling schemes,<sup>30</sup> and adaptive numerical integration.<sup>31</sup> Remarkably, besides electronic dynamics, TDCC theory also applies to nuclear dynamics<sup>32-34</sup> and vibrational problems.<sup>35,36</sup>

On the other hand, the Green's function (GF) approach<sup>37</sup> is often employed to treat electron correlation in excited electronic states. Electron correlation is crucial for determining and characterizing the quasiparticle (QP) and satellite peaks observed in, for example, X-ray photoemission spectra (XPS). To effectively capture this correlation in excited states, various theoretical approaches have incorporated the Green's function formulation. These include perturbative treatments,<sup>38-40</sup> algebraic diagrammatic construction,<sup>41-44</sup> dynamical mean-field theory,<sup>45,46</sup> GW approximations,<sup>47-50</sup> and ground state coupled cluster theory.<sup>51-58</sup>

Combining TDCC theory with Green's function formalism, Schönhammer and Gunnarsson have demonstrated the computation of the core-hole Green's function from the phase factors of the TDCC wave function.<sup>22</sup> Building on their formulation, we have recently developed a real-time equation-of-motion coupled cluster (RT-EOM-CC) cumulant GF approach,<sup>59-63</sup> in which the Green's function formulation adopts an exponential cumulant form to build up correlation in excited states, analogous to ground state coupled cluster theory. Technically, the cumulant is obtained by solving coupled ordinary differential equations of the TDCC amplitudes, providing higher-order vertex corrections to the one-particle self-energy compared to the traditional cumulant approximation<sup>54,64,65</sup> and the stochastic vertex approximation.<sup>66</sup> Numerical results have shown the applications of our RT-EOM-CC cumulant GF approach in reproducing the XPS of small-to-medium molecules described by moderate basis sets.<sup>61-63</sup> With heterogeneous parallel implementation and tensor algebraic techniques,

<sup>a)</sup>Electronic mail: peng398@pnnl.gov

RT-EOM-CC simulations of over 2,000 spin-orbitals have been achieved.<sup>67</sup>

While advancing towards larger-scale RT-EOM-CC simulations to resolve the many-body effects in the spectroscopy of more complex molecular systems, another fundamental aspect to consider is the exactness of the introduced TDCC ansatz in the computation of Green's functions and its alignment with the actual many-body physical picture of electron transitions. Our previous RT-EOM-CC results in computing spectral functions associated with QP and satellites, when compared with other theoretical approaches, show great agreement with experimental results. For instance, within the single and double excitation manifold, RT-EOM-CC results for some small molecules seemed more accurate than those obtained with CCGF using the modest basis set.<sup>61–63</sup> However, in weakly correlated scenarios within a single reference framework, CCGF can be exact in the expansion limit. It thus remains unclear whether the same exactness can be achieved with the RT-EOM-CC approach. Additionally, in previous treatments,<sup>22</sup> the TDCC ansatz was defined in the  $(N-1)$ -particle space, with the incorporation between the  $N$  and  $(N-1)$ -particle spaces approximated through the Hamiltonian transformation between different Fock spaces. In this paper, by explicitly considering both the  $N$  and  $(N-1)$ -particle spaces in the RT-EOM-CC cumulant GF approach, we examine the quality of the previous TDCC ansatz, and propose an enhanced new TDCC ansatz and its approximations that are based on the extended CC theory and are capable of incorporating different Fock spaces without the modification in the Hamiltonian. We then analyze the impact of different ansätze on the computed Green's functions. Moreover, we propose a scheme for addressing the component analysis of the Green's function computed by the RT-EOM-CC approach, which provides a powerful tool for characterization and peak assignment of the computed spectral functions. Our preliminary numerical test focuses on the single-impurity Anderson model (SIAM) with a limited number of bath sites, where high-level theoretical results and exact solutions can be obtained to test the performance and determine the exact limits of our proposed TDCC ansatz in RT-EOM-CC simulations.

## II. THEORY

### A. One-particle Green's function

The (retarded) one-particle Green's function at spin-orbital  $c$  is defined as

$$\begin{aligned} G_c^R(t) &= -i\Theta(t)\langle\Psi_c^{(N-1)}|e^{-i(H-E_g^{(N)})t}|\Psi_c^{(N-1)}\rangle \\ &= -i\Theta(t)e^{iE_g^{(N)}t}\langle\Psi^{(N)}|a_c^\dagger e^{-iHt}a_c|\Psi^{(N)}\rangle \end{aligned} \quad (1)$$

where  $H$  is the electronic Hamiltonian defined on the Fock space, and  $|\Psi_c^{(N-1)}\rangle$  is the  $(N-1)$ -electron state generated by removing one core electron at the spin-orbital  $|c\rangle$  from the  $N$ -electron ground state wave function  $|\Psi^{(N)}\rangle$ , i.e.  $|\Psi_c^{(N-1)}\rangle = a_c|\Psi^{(N)}\rangle$  with  $a_c$  and  $a_c^\dagger$  being the fermionic

annihilation and creation operators, respectively.  $E_g^{(N)}$  is the ground state energy of the  $N$ -electron system.

Employing the bi-orthogonal coupled cluster (CC) wave function ansatz<sup>51–53,55,68–79</sup> with respect to the  $N$ -electron single Slater determinant  $|\phi_0^{(N)}\rangle$

$$|\Psi^{(N)}\rangle = e^{T^{(N)}}|\phi_0^{(N)}\rangle; \quad (2)$$

$$\langle\Psi^{(N)}| = \langle\phi_0^{(N)}|(1 + \Lambda^{(N)})e^{-T^{(N)}}, \quad (3)$$

the one-particle Green's function can be rewritten as

$$\begin{aligned} G_c^R(t) &= -i\Theta(t)e^{iE_{CC}^{(N)}t} \times \\ &\langle\phi_0^{(N-1)}|(1 + L^{(N)})e^{-T^{(N)}}e^{-iHt}e^{T^{(N)}}|\phi_0^{(N-1)}\rangle. \end{aligned} \quad (4)$$

Here, the  $N$ -electron ground state energy  $E_g^{(N)}$  is replaced by the corresponding CC energy  $E_{CC}^{(N)}$ . The excitation and de-excitation CC operators,  $T^{(N)}$  and  $\Lambda^{(N)}$ , are defined as follows:

$$T^{(N)} = \sum_n t_n^{(N)}\mathbb{E}_n; \quad (5)$$

$$\Lambda^{(N)} = \sum_n l_n^{(N)}\mathbb{E}_n^\dagger \quad (6)$$

with  $t_n$ ,  $l_n$ , and  $s_n$  representing the amplitudes, and  $\mathbb{E}_n$  and  $\mathbb{E}_n^\dagger$  being the excitation and de-excitation generation operators, respectively. These operators are labeled by the compound index  $n$  for single, double, or higher order excitations. For example, for single and double excitations,

$$n^{(N)} = (p, q), \quad |n^{(N)}\rangle = \mathbb{E}_n|\phi_0^{(N)}\rangle = a_p^\dagger a_q|\phi_0^{(N)}\rangle;$$

$$n^{(N)} = (p, q, r, s), \quad |n^{(N)}\rangle = \mathbb{E}_n|\phi_0^{(N)}\rangle = a_p^\dagger a_q^\dagger a_r a_s|\phi_0^{(N)}\rangle,$$

here the indices  $p, q, r, s \dots$  label the spin-orbitals involved in the excitations. In Eq. (1), utilizing the commutative property  $[a_c, T^{(N)}] = 0$ , it follows that

$$|\Psi_c^{(N-1)}\rangle = a_c e^{T^{(N)}}|\phi_0^{(N)}\rangle = e^{T^{(N)}}|\phi_0^{(N-1)}\rangle \quad (7)$$

with  $|\phi_0^{(N-1)}\rangle = a_c|\phi_0^{(N)}\rangle$  being the  $(N-1)$ -electron single determinant. Throughout this paper, we use the subscript  $(N)$  or  $(N-1)$  in the operators for labeling the Hilbert space in which the operators are defined.

### B. Time-dependent equation-of-motion coupled cluster ansatz

In the previous time-dependent equation-of-motion coupled cluster (EOM-CC) ansatz,<sup>22,80</sup> the  $N$ -electron state  $|\Psi^{(N)}\rangle$ , and therefore the  $(N-1)$ -electron state at  $t=0$ ,  $|\Psi_c^{(N-1)}(0)\rangle = |\Psi_c^{(N-1)}\rangle$ , were assumed to be single Slater determinants. The time evolution of the  $(N-1)$ -electron state,  $|\Psi_c^{(N-1)}(t)\rangle$ , for any time  $t$ , is described by the following TDCC ansatz:

$$|\Psi_c^{(N-1)}(t)\rangle := N_c(t)e^{T^{(N-1)}(t)}|\Psi_c^{(N-1)}(0)\rangle, \quad (8)$$

where  $N_c(t)$  is a time-dependent normalization factor. The time-dependent CC operator  $T^{(N-1)}(t)$  in Eq. (8), defined in the  $(N-1)$ -particle space, includes transitions from the occupied spin-orbitals to the hole, which are absent in  $T^{(N)}$ .

Integrating the ansatz (8) into the time-dependent Schrödinger equation (TDSE) and after some reformulations, we derive the equations-of-motion (EOMs) for the normalization factor  $N_c(t)$  and the CC amplitudes  $t_n^{(N-1)}(t)$ :

$$\begin{aligned} i\partial \ln N_c(t)/\partial t &= \langle \Psi_c^{(N-1)}(0) | \bar{H}(t) | \Psi_c^{(N-1)}(0) \rangle \\ &= E_{CC}^{(N-1)}(t), \end{aligned} \quad (9)$$

$$i\partial t_n^{(N-1)}(t)/\partial t = \langle n^{(N-1)} | \bar{H}(t) | \Psi_c^{(N-1)}(0) \rangle, \quad (10)$$

where the time-dependent similarity transformed Hamiltonian  $\bar{H}(t) = e^{-T^{(N-1)}(t)} H e^{T^{(N-1)}(t)}$ . The one-particle Green's function is then expressed as

$$\begin{aligned} G_c^R(t) &= -i\Theta(t)N_c(t)e^{iE_{CC}^{(N-1)}t}O(t) \\ &= -i\Theta(t)\exp\left(\int_0^t -iE_{CC}^{(N-1)}(\tau)d\tau\right)e^{iE_{CC}^{(N-1)}t}O(t) \\ &= -i\Theta(t)\exp(-i\Delta E_{CC}(t)t)O(t). \end{aligned} \quad (11)$$

where

$$O(t) = \langle \phi_0^{(N)} | (1 + \Lambda^{(N)}) e^{-T^{(N)}} a_c^\dagger e^{T^{(N-1)}(t)} | \phi_0^{(N-1)} \rangle \quad (12)$$

and  $\Delta E_{CC}(t) = E_{CC}^{(N)} - [E_{CC}^{(N-1)}]_t$ . Here,  $[E_{CC}^{(N-1)}]_t$  denotes the time average of  $E_{CC}^{(N-1)}(\tau)$  over the period  $t$ , therefore we have

$$\exp\left(\int_0^t -iE_{CC}^{(N-1)}(\tau)d\tau\right) = \exp\left(-i[E_{CC}^{(N-1)}]_t t\right). \quad (13)$$

### C. Time-dependent extended coupled cluster ansatz

It is worthwhile to notice that correlation effects in the  $N$ -electron state, as described in the exact one-particle Green's function formulation Eq.(1), are approximated by directly considering the correlations in the  $(N-1)$ -electron state as seen in Eq. (8). This distinction can also be explicitly observed by comparing the ansätze in Eqs. (7) and (8). To enhance the description of correlation effects, particularly by incorporating correlations corresponding to the  $N$ -electron state, we propose more generalized time-dependent extended CC (eCC) ansatz

$$|\Psi_c^{(N-1)}(t)\rangle := \tilde{N}_c(t) e^{T^{(N)}} e^{T^{(N-1)}(t)} | \phi_0^{(N-1)} \rangle \quad (14)$$

with the initial conditions  $\tilde{N}_c(0) = 1$  and

$$|\Psi_c^{(N-1)}(0)\rangle = e^{T^{(N)}} | \phi_0^{(N-1)} \rangle \quad (15)$$

which reproduces ansatz (7). The difference in correlation level between the two ansätze (8) and (14) is summarized in Figure 1. Specifically, through the Taylor expansion of  $e^{T^{(N)}}$ , it is evident that the original ansatz (8) is the leading term of the ansatz (14). Consequently, the ansatz

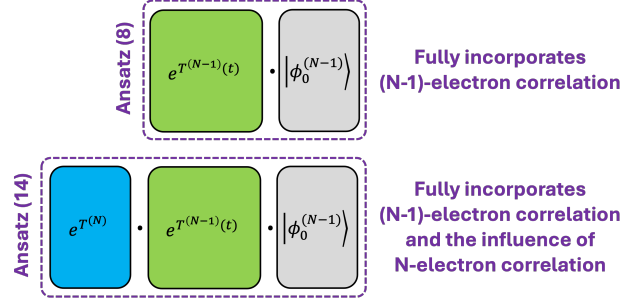


Figure 1. The comparison of ansatz (8) and (14) in terms of correlation level.

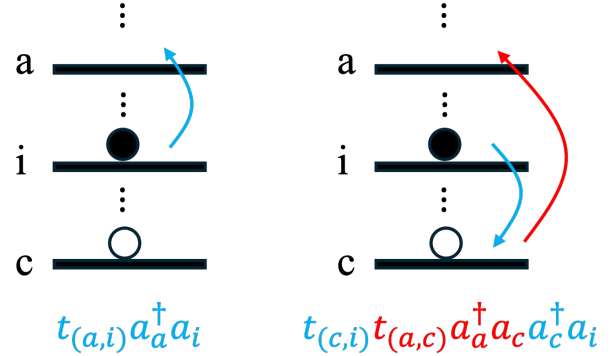


Figure 2. The schematic illustration of the excitation from an occupied spin-orbital  $i$  to a virtual spin-orbital  $a$  following the generation of a hole at spin-orbital  $c$ . The CC ansatz (8) is only able to describe the leading component of this excitation (left panel), while the extended CC ansatz (14) provides a higher order correction, mediated through a hole at spin-orbital  $c$  (right panel).

(14) is capable of capturing higher-order corrections to the excitation following the generation of a hole at spin-orbital  $c$ , as illustrated in Figure 2.

The new ansatz (14) bears resemblance to the double-unitary CC ansatz,<sup>81</sup> which incorporates two sets of excitation operators. When the ansatz (14) is applied to the time-dependent Schrödinger equation (TDSE), the EOMs for  $\tilde{N}_c(t)$  and  $t_n^{(N-1)}(t)$  are derived as follows:

$$\begin{aligned} i\partial \ln \tilde{N}_c(t)/\partial t &= \langle \phi_0^{(N-1)} | \bar{H}(t) | \phi_0^{(N-1)} \rangle \\ &= E_{eCC}^{(N-1)}(t), \end{aligned} \quad (16)$$

$$i\partial t_n^{(N-1)}(t)/\partial t = \langle n^{(N-1)} | \bar{H}(t) | \phi_0^{(N-1)} \rangle, \quad (17)$$

where the double similarity transformed Hamiltonian for the one-particle Green's function is defined as:

$$\bar{H}(t) = e^{-T^{(N-1)}(t)} e^{-T^{(N)}} H e^{T^{(N)}} e^{T^{(N-1)}(t)}. \quad (18)$$

It is important to note that Eqs. (16) and (17) depend on solving the  $N$ -electron CC equations for  $T^{(N)}$ , followed by the utilization of the ordinary differential equation (ODE) integrator for the  $(N-1)$ -electron state to propagate  $\tilde{N}_c(t)$  and  $t_n^{(N-1)}(t)$ . The workflow of the time propagation of the time-dependent  $(N-1)$ -electron correlated state described using the ansatz (14) is depicted in Figure 3. Consequently,

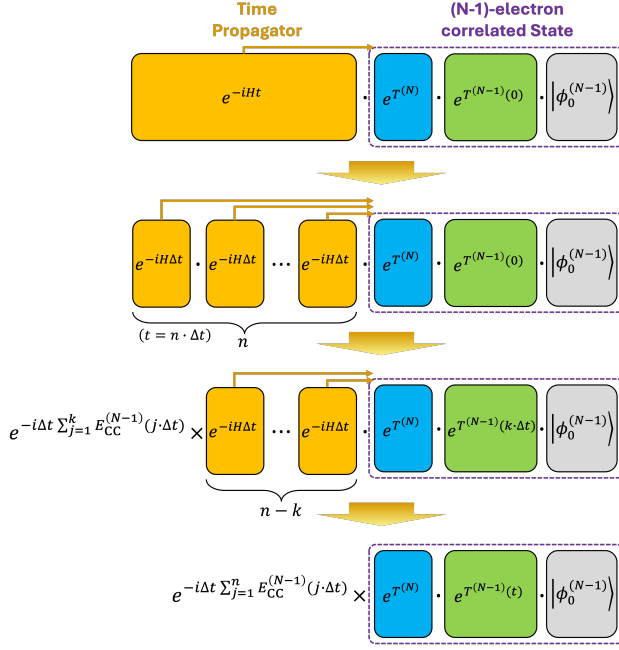


Figure 3. The schematic illustration of the new TDCC ansatz (14) and how it works to evaluate the time propagation of an  $(N-1)$ -electron correlated state.

the one-particle Green's function  $G_c^R(t)$  can be reformulated as:

$$G_c^R(t) = -i\Theta(t)\tilde{N}_c(t)e^{iE_{CC}^{(N)}t}O(t) \quad (19)$$

where

$$\tilde{N}_c(t) = \exp\left(-i[E_{CC}^{(N-1)}]_t t\right); \quad (20)$$

and the modified creation operator  $\overline{a_c^\dagger}$  is given by:

$$\overline{a_c^\dagger} = e^{-T^{(N)}}a_c^\dagger e^{T^{(N)}} = a_c^\dagger + [a_c^\dagger, T^{(N)}]. \quad (21)$$

The time-dependent overlap term  $O(t)$  is formulated as

$$O(t) = \langle \phi_0^{(N)} | (1 + \Lambda^{(N)}) \overline{a_c^\dagger} e^{T^{(N-1)}(t)} | \phi_0^{(N-1)} \rangle. \quad (22)$$

It is worth noting that the new ansatz (14) involves the product of two exponential operators, leading to double similarity transformation (18) in solving the EOMs (16) and (17). The double similarity transformation can potentially increase the non-linearity and leads to instability in the numerical propagation, thereby deteriorating the performance of the ODE integrator. In practical implementation, since the first similarity transformation,  $\tilde{H} = e^{-T^{(N)}} H e^{T^{(N)}}$  is time-independent, it can be computed upfront in the  $N$ -particle space before the time propagation in the  $(N-1)$ -particle space, with the computational cost paid for constructing  $\tilde{H}$ . Alternatively, the construction of  $\tilde{H}$  can be entirely avoided by employing approximate ansätze that combine the product of two exponential operators into one.

Straightforward approximations can be obtained by utilizing the Baker–Campbell–Hausdorff formula in (14) and

truncating the expansion at different (commutator) levels, for example:

$$|\Psi_c^{(N-1)}(t)\rangle \approx \tilde{N}_c(t) \times e^{T^{(N)}+T^{(N-1)}} |\phi_0^{(N-1)}\rangle, \quad (23)$$

$$|\Psi_c^{(N-1)}(t)\rangle \approx \tilde{N}_c(t) \times e^{T^{(N)}+T^{(N-1)}+\frac{1}{2}[T^{(N)},T^{(N-1)}]} |\phi_0^{(N-1)}\rangle, \quad (24)$$

⋮

The benefit of using the ansätze (23,24) in the EOMs (16 and 17) is to re-utilize the conventional CC implementation with modest modifications in the lists of the CC excitation operators. We will examine the numerical performance of such approximations in model systems in the following section.

#### D. Cluster analysis of $G_c^R$

It is important to note that the inclusion of  $O(t)$  in the formulation of  $G_c^R(t)$  causes the Fourier transform of  $G_c^R(t)$  to take a convolution form, i.e.,

$$G_c^R(\omega) \stackrel{t \rightarrow \infty}{\equiv} -i \int_{-\infty}^{\infty} \mathcal{F}\{O(t)\}(u) \delta(\omega - u - \Delta E) du = -i \mathcal{F}\{O(t)\}(\omega - \Delta E) \quad (25)$$

where

$$\Delta E = \lim_{t \rightarrow \infty} \left\{ E_{CC}^{(N)} - [E_{CC/eCC}^{(N-1)}]_t \right\} \quad (26)$$

approaches a constant scalar in the large  $t$  limit (due to  $\lim_{t \rightarrow \infty} [E_{CC/eCC}^{(N-1)}]_t = E_{CC}^{(N-1)}$ , see also Figure 4b,d below).  $\delta(\omega - u - \Delta E)$  is a Dirac delta function, and  $\mathcal{F}\{O(t)\}$  is the Fourier transform of  $O(t)$ :

$$\mathcal{F}\{O(t)\}(\omega) = \langle \phi_0^{(N)} | (1 + \Lambda^{(N)}) \overline{a_c^\dagger} \mathcal{F}\{e^{T^{(N-1)}(t)}\}(\omega) | \phi_0^{(N-1)} \rangle. \quad (27)$$

Furthermore, the expansion of  $e^{T^{(N-1)}(t)}$  is given by

$$\begin{aligned} e^{T^{(N-1)}(t)} &= e^{\sum_n t_n^{(N-1)}(t) \mathbb{E}_n} \\ &= \prod_n \left( 1 + t_n^{(N-1)}(t) \mathbb{E}_n \right) \\ &= 1 + \sum_n \tilde{t}_n^{(N-1)}(t) \mathbb{E}_n \end{aligned} \quad (28)$$

where the relationship between  $\tilde{t}_n^{(N-1)}(t)$  and  $t_n^{(N-1)}(t)$  can be determined through cluster analysis of Eq. (28). For example, if the CC operators only include the singles and doubles, we have:

$$\tilde{t}_{(p,q)}^{(N-1)}(t) = t_{(p,q)}^{(N-1)}(t), \quad (29)$$

$$\begin{aligned} \tilde{t}_{(p,q,r,s)}^{(N-1)}(t) &= t_{(p,q,r,s)}^{(N-1)}(t) + t_{(p,r)}^{(N-1)}(t) t_{(q,s)}^{(N-1)}(t) \\ &\quad - t_{(p,s)}^{(N-1)}(t) t_{(q,r)}^{(N-1)}(t). \end{aligned} \quad (30)$$

Therefore, in Eq. (27):

$$\mathcal{F}\{e^{T^{(N-1)}(t)}\}(\omega) = \delta(\omega) + \sum_n \mathcal{F}\{\tilde{t}_n^{(N-1)}\}(\omega)\mathbb{E}_n. \quad (31)$$

From Eqs. (25) and (31), the component analysis of the  $G_c^R(\omega)$  becomes straightforward.

### III. NUMERICAL RESULTS AND DISCUSSION

In this paper, we focus on evaluating the performance of our newly proposed ansatz for computing the one-particle Green's function in its exact limit. Particularly, we compare it with the performance of the previous ansatz. To this end, we employ the SIAM as our test framework within the RT-EOM-CC approach to compute the exact one-particle impurity Green's function. The SIAM Hamiltonian is expressed as follows:

$$H_{\text{SIAM}} = H_{\text{imp.}} + H_{\text{bath}} + H_{\text{hyb.}}, \quad (32)$$

where

$$H_{\text{imp.}} = \sum_{\sigma} \mu_c c_{\sigma}^{\dagger} c_{\sigma} + U c_{\uparrow}^{\dagger} c_{\uparrow} c_{\downarrow}^{\dagger} c_{\downarrow} \quad (33)$$

describes the impurity-site with potential  $\mu_c$  and the Coulomb interaction  $U$  between electrons with opposite spins ( $\sigma = \uparrow$  or  $\downarrow$ ) at the impurity site,

$$H_{\text{bath}} = \sum_{i=1, \sigma}^{N_b} \mu_{d,i} d_{i,\sigma}^{\dagger} d_{i,\sigma} \quad (34)$$

characterizes the non-interacting bath sites with potentials  $\mu_{d,i}$ 's, and

$$H_{\text{hyb.}} = \sum_{i=1, \sigma}^{N_b} V_i (c_{\sigma}^{\dagger} d_{i,\sigma} + d_{i,\sigma}^{\dagger} c_{\sigma}) \quad (35)$$

describes the coupling between the impurity site and the bath sites due to the hybridization. In subsequent tests, we focus on the three-site and four-site SIAM configurations, setting  $N = 4$ ,  $U = 3.0$  a.u.,  $\mu_c = -1.5$  a.u.,  $V_i = 0.5$  a.u.  $\forall i$ , and  $\mu_{d,i} \in [-1.0, 1.0]$  a.u.

#### A. Energy fluctuations of $(N-1)$ -electron states

We first evaluate the energy fluctuation of the  $(N-1)$ -electron state in the RT-EOM-CC simulations. For a three-site SIAM, as depicted in the inset of Figure 4b, since the highest level of excitations are double excitations, the exact propagation of the non-equilibrium  $(N-1)$ -electron state  $|\Psi_c^{(N-1)}\rangle$  can be accurately performed at the coupled cluster with singles and doubles (CCSD) level. Figure 4a illustrates the energy fluctuations of the  $(N-1)$ -electron state in RT-EOM-CCSD simulations using both the previous ansatz (8) and the new ansatz (14). In both ansatz, the CCSD operators are defined as:

$$\begin{aligned} T^{(N/N-1)} &= T_1^{(N/N-1)} + T_2^{(N/N-1)}, \\ \Lambda^{(N)} &= \Lambda_1^{(N)} + \Lambda_2^{(N)}. \end{aligned} \quad (36)$$

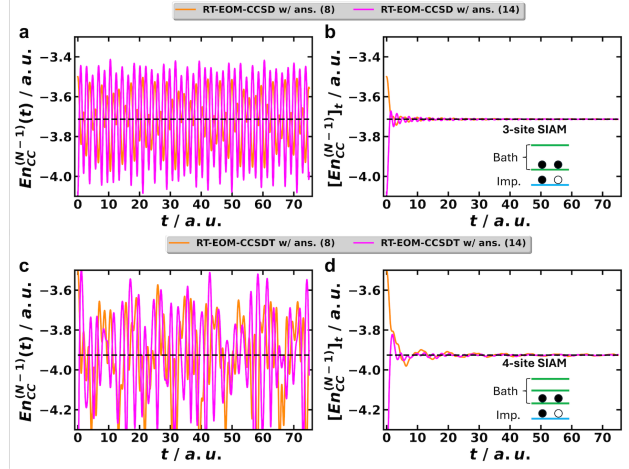


Figure 4. The energy fluctuation of the  $(N-1)$ -electron states of the three- and four-site SIAMs in the RT-EOM-CC simulations employing the ansatz (8) and (14). The reference state in the RT-EOM-CC simulations is a three-electron state (see the insets) where one electron resides at impurity site and two at the bath sites. In both cases, the time-average of the time-dependent  $(N-1)$ -electron energies,  $[E_{CC}^{(N-1)}]_t$ , converge to the stationary  $(N-1)$ -electron CC energies (denoted by the dashed lines),  $E_{CCSD}^{(N-1)}$  of  $-3.713370$  a.u. and  $E_{CCSDT}^{(N-1)}$  of  $-3.925962$  a.u., respectively, for the three- and four-site SIAMs.

Notably, the two RT-EOM-CCSD simulations have different energy starting points due to the choice of the ansatz. The starting energy in the simulation using ansatz (8) is the Hartree-Fock energy of the  $(N-1)$ -electron state, while the starting energy with ansatz (14) is considered to be that of a non-stationary  $(N-1)$ -electron correlated state. Additionally, as shown Figure 4b, although the time-dependent energy curves of the  $(N-1)$ -electron state vary between the two simulations, the time-averaged energies eventually converge to the same stationary  $(N-1)$ -electron CCSD energy of the half-filled three-site SIAM, irrespective of the ansatz used.

Figure 4c,d display the energy fluctuations in the RT-EOM-CCSDT simulations of the four-site SIAM. Due to the additional bath site compared to the three-site model, the CC operators in the exact limit are expanded as follows:

$$\begin{aligned} T^{(N)} &= T_1^{(N)} + T_2^{(N)} + T_3^{(N)} + T_4^{(N)}, \\ T^{(N-1)} &= T_1^{(N-1)} + T_2^{(N-1)} + T_3^{(N-1)}, \\ \Lambda^{(N)} &= \Lambda_1^{(N)} + \Lambda_2^{(N)} + \Lambda_3^{(N)} + \Lambda_4^{(N)}. \end{aligned} \quad (37)$$

Although the energy fluctuations are not as uniform as in the three-site model, the similar converging behavior of the time-averaged energies is observed, albeit over a slightly longer duration. It is worth noting that, with the selected parameters, the impact of quadruple excitations on the exact ground state of the four-site SIAM becomes negligible, therefore the exact ground state can be well approximated by the CCSDT wave function with an energy deviation  $< 2.0 \times 10^{-7}$  a.u.



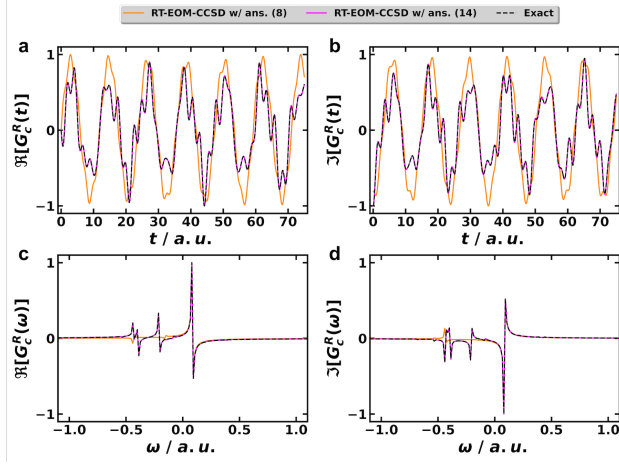


Figure 5. The impurity Green's functions,  $G_c^R(t)$  and  $G_c^R(\omega)$ , of the three-site SIAM ( $N = 4$ ) computed using the RT-EOM-CCSD approach employing the two ansatz (8) and (14). In the ansatz (14), the  $N$ -electron CC amplitude,  $T^{(N)}$ , is obtained from the  $N$ -electron CCSD calculation of the three-site SIAM. In the RT-EOM-CCSD simulation, the Runge-Kutta-Fehlberg approach, RK45, and its implementation in SciPy<sup>82</sup> were used in numerically solving the ODEs (10) and (17) for obtaining  $G_c^R(t)$  with  $t \in [0, 75]$  a.u. and  $\Delta t = 0.05$  a.u. Both  $G_c^R(t)$  and  $G_c^R(\omega)$  are normalized to be between  $[-1, 1]$ .

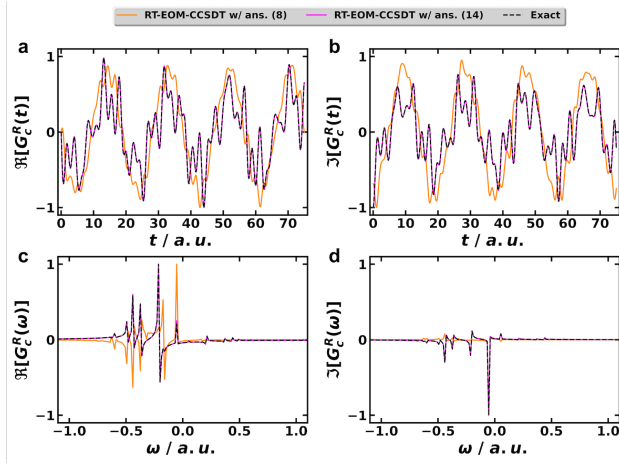


Figure 6. The impurity Green's functions,  $G_c^R(t)$  and  $G_c^R(\omega)$ , of the four-site SIAM ( $N = 4$ ) computed using the RT-EOM-CCSDT approach employing the two ansatz (8) and (14). In the ansatz (14), the  $N$ -electron CC amplitude,  $T^{(N)}$ , is obtained from the  $N$ -electron CCSDTQ calculation of the four-site SIAM. In the RT-EOM-CCSD simulation, the Runge-Kutta-Fehlberg approach, RK45, and its implementation in SciPy<sup>82</sup> were used in numerically solving the ODEs (10) and (17) for obtaining  $G_c^R(t)$  with  $t \in [0, 75]$  a.u. and  $\Delta t = 0.05$  a.u. Both  $G_c^R(t)$  and  $G_c^R(\omega)$  are normalized to be between  $[-1, 1]$ .

### B. $G_c^R$ computed through RT-EOM-CC with different ansatz

We then proceed to examine the computed  $G_c^R$  from the RT-EOM-CC approach using different ansatz. Figure 5 presents the impurity Green's function of the three-site SIAM, computed by the RT-EOM-CCSD approach em-

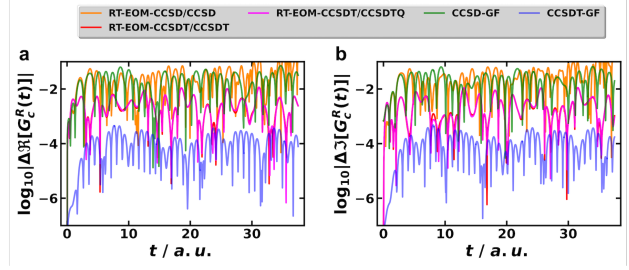


Figure 7. The deviation of the time-dependent impurity Green's functions,  $G_c^R(t)$ , from their exact values of the four-site SIAM ( $N = 4$ ) computed by different theoretical approaches. The exact values are obtained from the exact diagonalization of the Hamiltonian, and can also be equivalently obtained through CCSDTQ-GF calculations in the time domain. All the RT-EOM-CC simulations employ the ansatz (14), where the  $N$ -electron CC operators are obtained from converged CC ground state calculations with the convergence criteria of the energy change less than  $10^{-6}$  a.u. and the norm of the CC amplitude change less than  $10^{-7}$ . The Runge-Kutta-Fehlberg approach, RK45, and its implementation in SciPy<sup>82</sup> were used in numerically solving the ODEs (10) and (17) for obtaining  $G_c^R(t)$  with  $t \in [0, 37.5]$  a.u. and  $\Delta t = 0.05$  a.u.

ploying ansatz (8) and (14). For comparison, the exact  $G_c^R$  curves computed by Eq. (1) and exact diagonalization are also provided. As observed in Figure 5, the RT-EOM-CCSD simulation employing ansatz (14) successfully reproduces the exact  $G_c^R(t)$  curves, while the simulation using the ansatz (8) only captures a rough envelop of the exact time-propagation, missing the fine structure (i.e. the wiggles) of the exact curves. Consequently, after the Fourier transform, the curve obtained with ansatz (14) accurately reproduces both the main and satellite peaks, while the curves with ansatz (8) only capture the main peak at  $\omega \sim 0.1$  a.u.

The performance difference between the two ansatz (8) and (14) is further highlighted in Figure 6 when employing the RT-EOM-CCSDT approach for computing  $G_c^R(t)$  of the four-site SIAM. Notably, since the  $G_c^R(t)$  obtained using ansatz (8) does not strictly adhere to the envelope of the exact  $G_c^R(t)$ , its Fourier counterpart,  $G_c^R(\omega)$ , exhibits a slight shift in the main peak position. This shift is evident in Figure 6c, where the orange curve obtained with ansatz (8) deviates slightly from the exact main peak position at  $\sim -0.2$  a.u.

### C. Approaching the exact limit of $G_c^R$ in RT-EOM-CC simulations

To evaluate how closely the RT-EOM-CC approaches reach the exact limit, we closely examine the  $G_c^R(t)$  curves. Figure 7 illustrates the deviation of the  $G_c^R(t)$  obtained from the RT-EOM-CC simulations from the exact values, employing ansatz (14) across all simulations. The ground state CC approaches are explicitly mentioned in the Figure, because ansatz (14) also includes the  $N$ -electron CC operators obtained from the converged CC ground state calculations. Besides, we also include the CCSD-GF and CCSDT-GF results for comparison. Here, the CCGF values are obtained by substituting the CC left and right wave func-

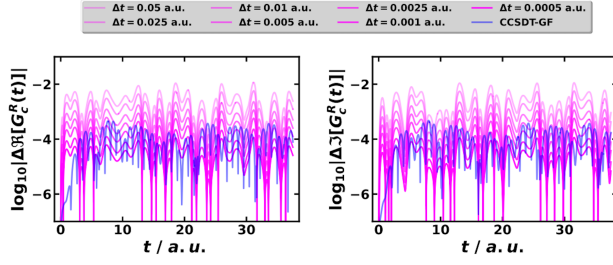


Figure 8. The deviation of the impurity Green's functions,  $G_c^R(t)$ , from the exact solution of the four-site SIAM ( $N = 4$ ) computed by the RT-EOM-CCSDT/CCSDTQ (with different time steps) and CCSDT-GF approaches. The exact solution is computed by the CCSDTQ-GF approach. All the RT-EOM-CC simulations employ the ansatz (14), where the  $N$ -electron CCSDTQ operators are obtained from converged CCSDTQ ground state calculations with the convergence criteria of energy change less than  $10^{-6}$  a.u. and the norm of the CC amplitude change less than  $10^{-7}$ . The Runge-Kutta-Fehlberg approach, RK45, and its implementation in SciPy were used in numerically solving the ODEs (10) and (17) for obtaining  $G_c^R(t)$  with  $t \in [0, 37.5]$  a.u. with different choices of time step.

tions,  $\langle \phi_0^{(N)} | (1 + \Lambda^{(N)}) e^{-T^{(N)}}$  and  $e^{T^{(N)}} | \phi_0^{(N)} \rangle$ , for  $\langle \Psi^{(N)} |$  and  $|\Psi^{(N)}\rangle$  in Eq. (1), respectively.

The simulations at the CCSD level, whether RT-EOM-CCSD or CCSD-GF, exhibit the largest deviations from the exact values among the employed approaches. Furthermore, the numerical stability of the employed ODE integrator becomes concerning when  $t > 35$  a.u. Within the RT-EOM-CC framework, there is an improvement of roughly one to two orders of magnitude from the RT-EOM-CCSD/CCSD results to the RT-EOM-CCSDT/CCSDT results, and the ODE integration becomes more stable for  $t > 35$  a.u. as observed in Figure 6. Adding the higher order excitations, the transition from RT-EOM-CCSDT/CCSDT results to RT-EOM-CCSDT/CCSDTQ results shows negligible change, even though the latter could be considered as approaching the exact limit of the RT-EOM-CC simulation for the four-site SIAM. By contrast, improvements in the CCGF approaches are consistent when increasing the excitation level to enhance the CC wave function. For instance, the CCSD-GF results are comparable in quality to the RT-EOM-CCSD/CCSD results, whereas the CCSDT-GF results clearly outperform the RT-EOM-CCSDT/CCSDTQ results, and the CCSDTQ-GF results numerically match the exact solution.

We attribute the deviation of the supposedly exact RT-EOM-CCSDT/CCSDTQ results to the discretization error caused by the finite size of the time step. To validate this hypothesis, we re-ran the RT-EOM-CCSDT/CCSDTQ simulations with varying time steps, and the results are depicted in Figure 8, with the CCSDT-GF results included for comparison. It is evident that as the time step decreases, the deviation of  $G_c^R(t)$  is consistently reduced, achieving and surpassing the accuracy level of the CCSDT-GF results for the four-site SIAM.

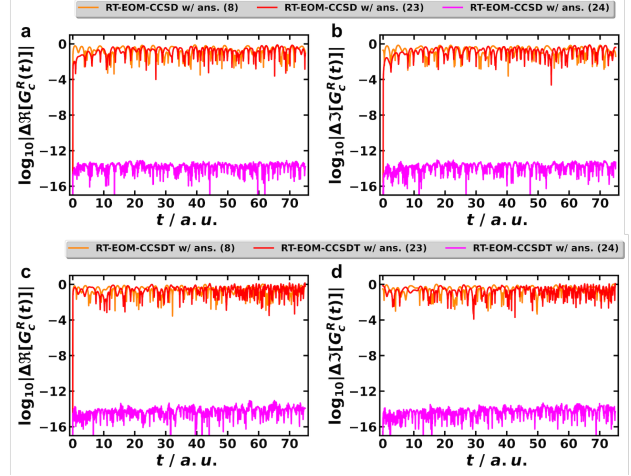


Figure 9. The deviation of  $G_c^R(t)$  of the four-site SIAM computed by RT-EOM-CCSDT with different approximate ansatz to the ansatz (14).

#### D. Computing $G_c^R$ using approximate ansatz in RT-EOM-CC simulations

In the previous sections, we demonstrated the performance differences between ansatz (8) and (14) and explored how to approach the exact limit of ansatz (14) in the RT-EOM-CC simulations of  $G_c^R(t)$  for the three- and four-site SIAMs. However, as discussed in Section II C, there may be challenges related to tensor operations and method implementation associated with the extended TDCC ansatz's algebraic structure and the tensor transition between the  $N$ - and  $(N - 1)$ -particle spaces. These challenges could, in the worst-case scenario, necessitate a redesign of the entire computational structure and library, adding another layer of complexity to realistic simulations.

To efficiently utilize the existing computational infrastructure, we introduce approximate ansatz, such as (23) and (24), in the RT-EOM-CC simulations to assess their efficacy. Figure 9 compares the performance of ansatz (8), (23), and (24) in the RT-EOM-CCSDT simulations of the four-site SIAM to that employing the ansatz (14). Here, we treat ansatz (8) as an approximation of ansatz (14) by assuming  $T^{(N)} = 0$ . The results show no significant performance difference between ansatz (8) and (23). However, incorporating the single commutator between  $T^{(N)}$  and  $T^{(N-1)}$  in the exponent to generate ansatz (24) leads to a marked improvement. It's noteworthy that the single commutator introduces higher order corrections in the exponential operators, such that

$$e^{T^{(N)} + T^{(N-1)} + \frac{1}{2}[T^{(N)}, T^{(N-1)}]} | \phi_0^{(N-1)} \rangle = e^{T^{(N)}} e^{T^{(N-1)}} | \phi_0^{(N-1)} \rangle \quad (38)$$

for the four-site SIAM, explaining the minimal deviations observed with ansatz (24) in Figure 9.

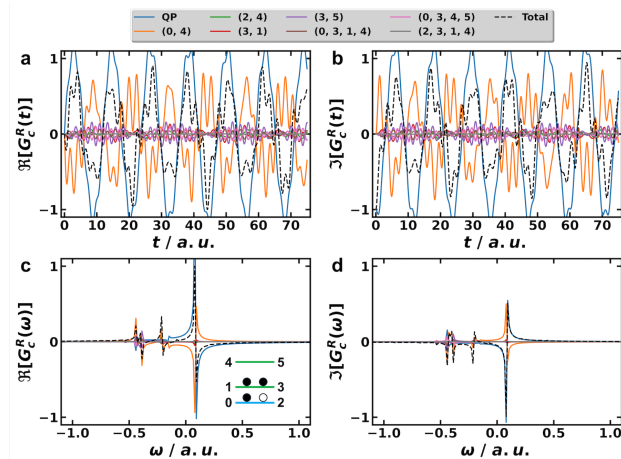


Figure 10. The component analysis of the impurity Green's functions,  $G_c^R(t)$  and  $G_c^R(\omega)$ , of the three-site SIAM. The inset in (c) shows the labeling of the spin-orbitals in the three-site SIAM.

### E. Component analysis of $G_c^R$

Finally, we demonstrate the component analysis on the  $G_c^R$  of the three-site SIAM employing the approach described in Section II D. The analysis implicitly assumes the large  $t$  limit, which is justified by the observation in Figure 4b, where Eq. (26) essentially represents the energy difference between  $N$ - and  $(N-1)$ -electron stationary states. Figure 10 presents the component analysis of the  $G_c^R(t)$  and  $G_c^R(\omega)$  using Eqs. (25)-(31). As observed, in addition to the main QP peak (at  $\sim 0.1$  a.u.), significant contributions to the satellite peaks between  $-0.5$  and  $0.0$  a.u. are provided by the single excitations from the impurity site to the bath site ( $0 \rightarrow 4$ ), from one bath site to another ( $3 \rightarrow 5$ ), and the double excitation ( $0, 3 \rightarrow 4, 5$ ).

## IV. CONCLUSION AND OUTLOOK

In the paper, we have analyzed and examined a series of TDCC ansätze in the RT-EOM-CC simulations for computing the one-particle Green's function. Unlike the previously used TDCC ansatz used in RT-EOM-CC simulations, we introduced a new TDCC ansatz that features an extended CC form—the product of the exponential CC operators from  $N$  and  $(N-1)$ -particle spaces. Preliminary analysis and simulations on simple SIAMs demonstrate that, compared to the previous TDCC ansatz, the new one is capable of approaching the exact limit by incorporating higher order excitations in the  $(N-1)$ -electron CC exponential operator and by using small time steps. By employing the BCH expansion of the new ansatz and truncating at different commutator levels, we have also introduced some approximate TDCC ansätze to the RT-EOM-CC simulations. The approximate ansätze feature a single exponential algebraic structure that potentially balances the complexity of implementation with accuracy. Additionally, we have formalized a recipe for analyzing the components of the computed Green's function in RT-EOM-CC simulations, paving the way for larger-scale and efficient implementations and detailed spectral function

analysis for complex molecular systems in the near future. Future work will focus on incorporating the double-unitary CC ansätze<sup>81</sup> into the RT-EOM-CC framework, extending RT-EOM-CC to compute the nonequilibrium Green's function,<sup>28,29</sup> and improving numerical aspects including more stable ODE integrator<sup>83</sup> and robust interpolation and extrapolation techniques<sup>84,85</sup>.

## V. ACKNOWLEDGEMENTS

This material is based upon work supported by the “Transferring exascale computational chemistry to cloud computing environment and emerging hardware technologies (TEC<sup>4</sup>)” project, which is funded by the U.S. Department of Energy, Office of Science, Office of Basic Energy Sciences, the Division of Chemical Sciences, Geosciences, and Biosciences (under FWP 82037). F.D.V and J.J.R. acknowledge the support from the Center for Scalable Predictive methods for Excitations and Correlated phenomena (SPEC), which is funded by the U.S. Department of Energy (DoE), Office of Science, Office of Basic Energy Sciences, Division of Chemical Sciences, Geosciences and Biosciences as part of the Computational Chemical Sciences (CCS) program at Pacific Northwest National Laboratory (PNNL) under FWP 70942. B.P. also acknowledges Dr. Niri Govind for the fruitful discussion during the preparation of the manuscript.

## REFERENCES

- <sup>1</sup>M. Isinger, R. J. Squibb, D. Busto, S. Zhong, A. Harth, D. Kroon, S. Nandi, C. L. Arnold, M. Miranda, J. M. Dahlström, E. Lindroth, R. Feifel, M. Gisselbrecht, and A. L'Huillier, “Photoionization in the time and frequency domain,” *Science* **358**, 893–896 (2017).
- <sup>2</sup>M. Schultze, M. Fieß, N. Karpowicz, J. Gagnon, M. Korbman, M. Hofstetter, S. Neppl, A. L. Cavalieri, Y. Komninos, T. Mercouris, C. A. Nicolaides, R. Pazourek, S. Nagele, J. Feist, J. Burgdörfer, A. M. Azzeer, R. Ernstorfer, R. Kienberger, U. Kleineberg, E. Goulielmakis, F. Krausz, and V. S. Yakovlev, “Delay in photoemission,” *Science* **328**, 1658–1662 (2010).
- <sup>3</sup>M. Huppert, I. Jordan, D. Baykusheva, A. von Conta, and H. J. Wörner, “Attosecond delays in molecular photoionization,” *Phys. Rev. Lett.* **117**, 093001 (2016).
- <sup>4</sup>E. Goulielmakis, Z.-H. Loh, A. Wirth, R. Santra, N. Rohringer, V. S. Yakovlev, S. Zherebtsov, T. Pfeifer, A. M. Azzeer, M. F. Kling, S. R. Leone, and F. Krausz, “Real-time observation of valence electron motion,” *Nature* **466**, 739–743 (2010).
- <sup>5</sup>P. M. Kraus, B. Mignolet, D. Baykusheva, A. Rupenyana, L. Horný, E. F. Penka, G. Grassi, O. I. Tolstikhin, J. Schneider, F. Jensen, L. B. Madsen, A. D. Bandrauk, F. Remacle, and H. J. Wörner, “Measurement and laser control of attosecond charge migration in ionized iodoacetylene,” *Science* **350**, 790–795 (2015).
- <sup>6</sup>S. Li, L. Lu, S. Bhattacharyya, C. Pearce, K. Li, E. T. Nienhuis, G. Doumy, R. D. Schaller, S. Moeller, M.-F. Lin, G. Dakovski, D. J. Hoffman, D. Garratt, K. A. Larsen, J. D. Koralek, C. Y. Hampton, D. Cesar, J. Duris, Z. Zhang, N. Sudar, J. P. Cryan, A. Marinelli, X. Li, L. Inhester, R. Santra, and L. Young, “Attosecond-pump attosecond-probe x-ray spectroscopy of liquid water,” *Science* **383**, 1118–1122 (2024).
- <sup>7</sup>G. Sansone, F. Kelkensberg, J. F. Pérez-Torres, F. Morales, M. F. Kling, W. Siu, O. Ghafur, P. Johnsson, M. Swoboda, E. Benedetti, F. Ferrari, F. Lépine, J. L. Sanz-Vicario, S. Zherebtsov, I. Znakovskaya, A. L'Huillier, M. Y. Ivanov, M. Nisoli, F. Martín, and M. J. J. Vrakking, “Electron localization following attosecond molecular photoionization,” *Nature* **465**, 763–766 (2010).



- <sup>8</sup>F. Calegari, D. Ayuso, A. Trabattini, L. Belshaw, S. D. Camillis, S. Anumula, F. Frassetto, L. Poletto, A. Palacios, P. Declava, J. B. Greenwood, F. Martín, and M. Nisoli, "Ultrafast electron dynamics in phenylalanine initiated by attosecond pulses," *Science* **346**, 336–339 (2014).
- <sup>9</sup>C. Ott, A. Kaldun, P. Raith, K. Meyer, M. Laux, J. Evers, C. H. Keitel, C. H. Greene, and T. Pfeifer, "Lorentz meets fano in spectral line shapes: A universal phase and its laser control," *Science* **340**, 716–720 (2013).
- <sup>10</sup>M. Schultze, E. M. Bothschafter, A. Sommer, S. Holzner, W. Schweinberger, M. Fiess, M. Hofstetter, R. Kienberger, V. Apalkov, V. S. Yakovlev, M. I. Stockman, and F. Krausz, "Controlling dielectrics with the electric field of light," *Nature* **493**, 75–78 (2013).
- <sup>11</sup>X. Li, N. Govind, C. Isborn, A. E. I. DePrince, and K. Lopata, "Real-time time-dependent electronic structure theory," *Chem. Rev.* **120**, 9951–9993 (2020), pMID: 32813506.
- <sup>12</sup>H.-D. Meyer, U. Manthe, and L. Cederbaum, "The multi-configurational time-dependent hartree approach," *Chem. Phys. Lett.* **165**, 73–78 (1990).
- <sup>13</sup>M. Beck, A. Jäckle, G. Worth, and H.-D. Meyer, "The multiconfiguration time-dependent hartree (mctdh) method: a highly efficient algorithm for propagating wavepackets," *Phys. Rep.* **324**, 1–105 (2000).
- <sup>14</sup>H.-D. Meyer and G. A. Worth, "Quantum molecular dynamics: propagating wavepackets and density operators using the multiconfiguration time-dependent hartree method," *Theo. Chem. Acc.* **109**, 251–267 (2003).
- <sup>15</sup>T. Sato and K. L. Ishikawa, "Time-dependent complete-active-space self-consistent-field method for multielectron dynamics in intense laser fields," *Phys. Rev. A* **88**, 023402 (2013).
- <sup>16</sup>H. Miyagi and L. B. Madsen, "Time-dependent restricted-active-space self-consistent-field theory for laser-driven many-electron dynamics," *Phys. Rev. A* **87**, 062511 (2013).
- <sup>17</sup>S. Bauch, L. K. Sørensen, and L. B. Madsen, "Time-dependent generalized-active-space configuration-interaction approach to photoionization dynamics of atoms and molecules," *Phys. Rev. A* **90**, 062508 (2014).
- <sup>18</sup>H. J. Monkhorst, "Calculation of properties with the coupled-cluster method," *Int. J. Quantum Chem.* **12**, 421–432 (1977).
- <sup>19</sup>E. Dalgaard and H. J. Monkhorst, "Some aspects of the time-dependent coupled-cluster approach to dynamic response functions," *Phys. Rev. A* **28**, 1217–1222 (1983).
- <sup>20</sup>B. Sverdrup Ofstad, E. Aurbakken, O. Sigmundson Schøyen, H. E. Kristiansen, S. Kvaal, and T. B. Pedersen, "Time-dependent coupled-cluster theory," *WIREs Comput. Mol. Sci.* **13**, e1666 (2023).
- <sup>21</sup>M. Takahashi and J. Paldus, "Time-dependent coupled cluster approach: Excitation energy calculation using an orthogonally spin-adapted formalism," *J. Chem. Phys.* **85**, 1486–1501 (1986).
- <sup>22</sup>K. Schönhammer and O. Gunnarsson, "Time-dependent approach to the calculation of spectral functions," *Phys. Rev. B* **18**, 6606–6614 (1978).
- <sup>23</sup>D. R. Nascimento and A. E. I. DePrince, "Linear absorption spectra from explicitly time-dependent equation-of-motion coupled-cluster theory," *J. Chem. Theory Comput.* **12**, 5834–5840 (2016), pMID: 27779862.
- <sup>24</sup>D. R. Nascimento and I. DePrince, A. Eugene, "A general time-domain formulation of equation-of-motion coupled-cluster theory for linear spectroscopy," *J. Chem. Phys.* **151**, 204107 (2019).
- <sup>25</sup>D. R. Nascimento and A. E. I. DePrince, "Simulation of near-edge x-ray absorption fine structure with time-dependent equation-of-motion coupled-cluster theory," *J. Phys. Chem. Lett.* **8**, 2951–2957 (2017), pMID: 28609098.
- <sup>26</sup>A. S. Skeidsvoll, A. Balbi, and H. Koch, "Time-dependent coupled-cluster theory for ultrafast transient-absorption spectroscopy," *Phys. Rev. A* **102**, 023115 (2020a).
- <sup>27</sup>L. N. Koulias, D. B. Williams-Young, D. R. Nascimento, A. E. I. DePrince, and X. Li, "Relativistic real-time time-dependent equation-of-motion coupled-cluster," *J. Chem. Theory Comput.* **15**, 6617–6624 (2019), pMID: 31618584.
- <sup>28</sup>A. F. White and G. K.-L. Chan, "A time-dependent formulation of coupled-cluster theory for many-fermion systems at finite temperature," *J. Chem. Theory Comput.* **14**, 5690–5700 (2018), pMID: 30260642.
- <sup>29</sup>A. F. White and G. K.-L. Chan, "Time-dependent coupled cluster theory on the keldysh contour for nonequilibrium systems," *J. Chem. Theory Comput.* **15**, 6137–6153 (2019), pMID: 31600075.
- <sup>30</sup>B. G. Peyton, Z. Wang, and T. D. Crawford, "Reduced scaling real-time coupled cluster theory," *J. Phys. Chem. A* **127**, 8486–8499 (2023), pMID: 37782945.
- <sup>31</sup>Z. Wang, B. G. Peyton, and T. D. Crawford, "Accelerating real-time coupled cluster methods with single-precision arithmetic and adaptive numerical integration," *J. Chem. Theory Comput.* **18**, 5479–5491 (2022), pMID: 35939815.
- <sup>32</sup>P. Hoodbhoy and J. W. Negele, "Time-dependent coupled-cluster approximation to nuclear dynamics. i. application to a solvable model," *Phys. Rev. C* **18**, 2380–2394 (1978).
- <sup>33</sup>P. Hoodbhoy and J. W. Negele, "Time-dependent coupled-cluster approximation to nuclear dynamics. ii. general formulation," *Phys. Rev. C* **19**, 1971–1982 (1979).
- <sup>34</sup>D. A. Pigg, G. Hagen, H. Nam, and T. Papenbrock, "Time-dependent coupled-cluster method for atomic nuclei," *Phys. Rev. C* **86**, 014308 (2012).
- <sup>35</sup>S. Bao, N. Raymond, and M. Nooijen, "Time dependent vibrational electronic coupled cluster (VECC) theory for non-adiabatic nuclear dynamics," *J. Chem. Phys.* **160**, 094105 (2024).
- <sup>36</sup>M. G. Højlund, A. Zocante, and O. Christiansen, "Time-dependent coupled cluster with orthogonal adaptive basis functions: General formalism and application to the vibrational problem," *J. Chem. Phys.* **160**, 024105 (2024).
- <sup>37</sup>L. Hedin, "On correlation effects in electron spectroscopies and the GW approximation," *J. Phys.: Condens. Matter* **11**, R489 (1999).
- <sup>38</sup>J. J. Phillips and D. Zgid, "Communication: The description of strong correlation within self-consistent Green's function second-order perturbation theory," *J. Chem. Phys.* **140**, 241101 (2014).
- <sup>39</sup>S. Hirata, A. E. Doran, P. J. Knowles, and J. V. Ortiz, "One-particle many-body Green's function theory: Algebraic recursive definitions, linked-diagram theorem, irreducible-diagram theorem, and general-order algorithms," *J. Chem. Phys.* **147**, 044108 (2017).
- <sup>40</sup>N. E. Dahlen and R. van Leeuwen, "Self-consistent solution of the Dyson equation for atoms and molecules within a conserving approximation," *J. Chem. Phys.* **122**, 164102 (2005).
- <sup>41</sup>J. Schirmer, "Beyond the random-phase approximation: A new approximation scheme for the polarization propagator," *Phys. Rev. A* **26**, 2395–2416 (1982).
- <sup>42</sup>J. Schirmer, L. S. Cederbaum, and O. Walter, "New approach to the one-particle green's function for finite fermi systems," *Phys. Rev. A* **28**, 1237–1259 (1983).
- <sup>43</sup>A. Drew and M. Wormit, "The algebraic diagrammatic construction scheme for the polarization propagator for the calculation of excited states," *WIREs Comput. Mol. Sci.* **5**, 82–95 (2015).
- <sup>44</sup>S. Banerjee and A. Y. Sokolov, "Third-order algebraic diagrammatic construction theory for electron attachment and ionization energies: Conventional and Green's function implementation," *J. Chem. Phys.* **151**, 224112 (2019).
- <sup>45</sup>A. Georges, G. Kotliar, W. Krauth, and M. J. Rozenberg, "Dynamical mean-field theory of strongly correlated fermion systems and the limit of infinite dimensions," *Rev. Mod. Phys.* **68**, 13–125 (1996).
- <sup>46</sup>G. Kotliar, S. Y. Savrasov, K. Haule, V. S. Oudovenko, O. Parcollet, and C. A. Marianetti, "Electronic structure calculations with dynamical mean-field theory," *Rev. Mod. Phys.* **78**, 865–951 (2006).
- <sup>47</sup>L. Hedin, "New method for calculating the one-particle green's function with application to the electron-gas problem," *Phys. Rev.* **139**, A796–A823 (1965).
- <sup>48</sup>F. Aryasetiawan and O. Gunnarsson, "The gw method," *Rep. Prog. Phys.* **61**, 237 (1998).
- <sup>49</sup>M. van Schilfhaarde, T. Kotani, and S. Faleev, "Quasiparticle self-consistent gw theory," *Phys. Rev. Lett.* **96**, 226402 (2006).
- <sup>50</sup>P. Koval, D. Foerster, and D. Sánchez-Portal, "Fully self-consistent gw and quasiparticle self-consistent gw for molecules," *Phys. Rev. B* **89**, 155417 (2014).
- <sup>51</sup>M. Nooijen and J. G. Snijders, "Coupled cluster approach to the single-particle green's function," *Int. J. Quantum Chem.* **44**, 55–83 (1992).
- <sup>52</sup>M. Nooijen and J. G. Snijders, "Coupled cluster green's function method: Working equations and applications," *Int. J. Quantum Chem.* **48**, 15–48 (1993).
- <sup>53</sup>M. Nooijen and J. G. Snijders, "Second order many-body perturbation approximations to the coupled cluster green's function," *J. Chem. Phys.* **102**, 1681–1688 (1995).
- <sup>54</sup>J. McClain, J. Lischner, T. Watson, D. A. Matthews, E. Ronca, S. G. Louie, T. C. Berkelbach, and G. K.-L. Chan, "Spectral functions of the uniform electron gas via coupled-cluster theory and comparison to the gw and related approximations," *Phys. Rev. B* **93**, 235139 (2016).

- <sup>55</sup>B. Peng and K. Kowalski, “Green’s function coupled-cluster approach: Simulating photoelectron spectra for realistic molecular systems,” *J. Chem. Theory Comput.* **14**, 4335–4352 (2018).
- <sup>56</sup>M. Lange and T. Berkelbach, “On the relation between equation-of-motion coupled-cluster theory and the gw approximation,” *J. Chem. Theory Comput.* **14**, 4224–4236 (2018).
- <sup>57</sup>T. Zhu, C. A. Jiménez-Hoyos, J. McClain, T. C. Berkelbach, and G. K.-L. Chan, “Coupled-cluster impurity solvers for dynamical mean-field theory,” *Phys. Rev. B* **100**, 115154 (2019).
- <sup>58</sup>A. Shee and D. Zgid, “Coupled cluster as an impurity solver for green’s function embedding methods,” *J. Chem. Theory Comput.* **15**, 6010–6024 (2019).
- <sup>59</sup>J. J. Rehr, F. D. Vila, J. J. Kas, N. Y. Hirshberg, K. Kowalski, and B. Peng, “Equation of motion coupled-cluster cumulant approach for intrinsic losses in x-ray spectra,” *J. Chem. Phys.* **152**, 174113 (2020).
- <sup>60</sup>F. D. Vila, J. J. Rehr, J. J. Kas, K. Kowalski, and B. Peng, “Real-time coupled-cluster approach for the cumulant green’s function,” *J. Chem. Theory Comput.* **16**, 6983–6992 (2020).
- <sup>61</sup>F. D. Vila, J. J. Kas, J. J. Rehr, K. Kowalski, and B. Peng, “Equation-of-motion coupled-cluster cumulant green’s function for excited states and x-ray spectra,” *Front. Chem.* **9**, 734945 (2021).
- <sup>62</sup>F. Vila, K. Kowalski, B. Peng, J. Kas, and J. Rehr, “Real-time equation-of-motion ccSD cumulant green’s function,” *J. Chem. Theory Comput.* **18**, 1799–1807 (2022).
- <sup>63</sup>F. Vila, J. Rehr, H. Pathak, B. Peng, A. Panyala, E. Mutlu, N. Bauman, and K. Kowalski, “Real-time equation-of-motion cc cumulant and cc green’s function simulations of photoemission spectra of water and water dimer,” *J. Chem. Phys.* **157**, 044101 (2022).
- <sup>64</sup>J. S. Zhou, J. J. Kas, L. Sponza, I. Reshetnyak, M. Guzzo, C. Giorgetti, M. Gatti, F. Sottile, J. J. Rehr, and L. Reining, “Dynamical effects in electron spectroscopy,” *J. Chem. Phys.* **143**, 184109 (2015).
- <sup>65</sup>L. Hedin, “On correlation effects in electron spectroscopies and the gw approximation,” *J. Phys. Cond. Matt.* **11**, R489 (1999).
- <sup>66</sup>C. Mejuto-Zaera, G. Weng, M. Romanova, S. J. Cotton, K. B. Whaley, N. M. Tubman, and V. Vlček, “Are multi-quasiparticle interactions important in molecular ionization?” *J. Chem. Phys.* **154**, 121101 (2021).
- <sup>67</sup>H. Pathak, A. Panyala, B. Peng, N. P. Bauman, E. Mutlu, J. J. Rehr, F. D. Vila, and K. Kowalski, “Real-time equation-of-motion coupled-cluster cumulant green’s function method: Heterogeneous parallel implementation based on the tensor algebra for many-body methods infrastructure,” *J. Chem. Theory Comput.* **19**, 2248–2257 (2023), pMID: 37096369.
- <sup>68</sup>J. Arponen, “Variational principles and linked-cluster expansion for static and dynamic many-body problems,” *Ann. Phys.* **151**, 311–382 (1983).
- <sup>69</sup>P. G. Szalay, M. Nooijen, and R. J. Bartlett, “Alternative ansätze in single reference coupled-cluster theory. iii. a critical analysis of different methods,” *J. Chem. Phys.* **103**, 281–298 (1995).
- <sup>70</sup>P. Piecuch and R. J. Bartlett, “Eomcc: A new coupled-cluster method for electronic excited states,” *Adv. Quantum Chem.* **34**, 295–380 (1999).
- <sup>71</sup>E. A. Salter, H. Sekino, and R. J. Bartlett, “Property evaluation and orbital relaxation in coupled cluster methods,” *J. Chem. Phys.* **87**, 502–509 (1987).
- <sup>72</sup>J. F. Stanton and R. J. Bartlett, “The equation of motion coupled-cluster method. a systematic biorthogonal approach to molecular excitation energies, transition probabilities, and excited state properties,” *J. Chem. Phys.* **98**, 7029–7039 (1993).
- <sup>73</sup>H. J. Monkhorst, “Calculation of properties with the coupled-cluster method,” *Int. J. Quantum Chem.* **12**, 421–432 (1977).
- <sup>74</sup>H. Koch and P. Jørgensen, “Coupled cluster response functions,” *J. Chem. Phys.* **93**, 3333–3344 (1990).
- <sup>75</sup>K. Kowalski, K. Bhaskaran-Nair, and W. A. Shelton, “Coupled-cluster representation of green function employing modified spectral resolutions of similarity transformed hamiltonians,” *J. Chem. Phys.* **141**, 094102 (2014).
- <sup>76</sup>K. Bhaskaran-Nair, K. Kowalski, and W. A. Shelton, “Coupled cluster green function: Model involving single and double excitations,” *J. Chem. Phys.* **144**, 144101 (2016).
- <sup>77</sup>B. Peng and K. Kowalski, “Coupled-cluster green’s function: Analysis of properties originating in the exponential parametrization of the ground-state wave function,” *Phys. Rev. A* **94**, 062512 (2016).
- <sup>78</sup>T. Helgaker, P. Jørgensen, and J. Olsen, *Molecular Electronic-Structure Theory* (Wiley, 2014).
- <sup>79</sup>J. Schirmer and F. Mertins, “Review of biorthogonal coupled cluster representations for electronic excitation,” *Theor. Chem. Acc* **125**, 145–172 (2010).
- <sup>80</sup>J. J. Rehr, F. D. Vila, J. J. Kas, N. Y. Hirshberg, K. Kowalski, and B. Peng, “Equation of motion coupled-cluster cumulant approach for intrinsic losses in x-ray spectra,” *J. Chem. Phys.* **152**, 174113 (2020).
- <sup>81</sup>N. P. Bauman, E. J. Bylaska, S. Krishnamoorthy, G. H. Low, N. Wiebe, C. E. Granade, M. Roetteler, M. Troyer, and K. Kowalski, “Downfolding of many-body Hamiltonians using active-space models: Extension of the sub-system embedding sub-algebras approach to unitary coupled cluster formalisms,” *J. Chem. Phys.* **151**, 014107 (2019).
- <sup>82</sup>P. Virtanen, R. Gommers, T. E. Oliphant, M. Haberland, T. Reddy, D. Cournapeau, E. Burovski, P. Peterson, W. Weckesser, J. Bright, S. J. van der Walt, M. Brett, J. Wilson, K. J. Millman, N. Mayorov, A. R. J. Nelson, E. Jones, R. Kern, E. Larson, C. J. Carey, Í. Polat, Y. Feng, E. W. Moore, J. VanderPlas, D. Laxalde, J. Perktold, R. Cimrman, I. Henriksen, E. A. Quintero, C. R. Harris, A. M. Archibald, A. H. Ribeiro, F. Pedregosa, P. van Mulbregt, and SciPy 1.0 Contributors, “SciPy 1.0: Fundamental Algorithms for Scientific Computing in Python,” *Nature Methods* **17**, 261–272 (2020).
- <sup>83</sup>D. B. Williams-Young, S. H. Yuwono, A. E. DePrince III, and C. Yang, “Approximate exponential integrators for time-dependent equation-of-motion coupled cluster theory,” *J. Chem. Theory Comput.* **19**, 9177–9186 (2023), pMID: 38086060.
- <sup>84</sup>B. Peng, R. Van, Beeumen, D. B. Williams-Young, K. Kowalski, and C. Yang, “Approximate green’s function coupled cluster method employing effective dimension reduction,” *J. Chem. Theory Comput.* **15**, 3185–3196 (2019).
- <sup>85</sup>C. C. Reeves, J. Yin, Y. Zhu, K. Z. Ibrahim, C. Yang, and V. c. v. Vlček, “Dynamic mode decomposition for extrapolating nonequilibrium green’s-function dynamics,” *Phys. Rev. B* **107**, 075107 (2023).